Pressure-Induced New Topological Weyl Semimetal Phase in TaAs

Yonghui Zhou, Pengchao Lu, Yongping Du, Xiangde Zhu, Ganghua Zhang, Ranran Zhang, Dexi Shao, Xuliang Chen, Xuefei Wang, Mingliang Tian, Jian Sun, Xiangang Wan, Zhaorong Yang, Wenge Yang, Yuheng Zhang, and Dingyu Xing

Phys. Rev. Lett. **117**, 146402 — Published 28 September 2016
DOI: 10.1103/PhysRevLett.117.146402

Pressure-induced new topological Weyl Semimetal phase in TaAs

Yonghui Zhou,[1,2,*] Pengchao Lu,[3,*] Yongping Du,[3,*] Xiangde Zhu,[1,*] Ganghua Zhang,[4] Ranran Zhang,[1] Dexi Shao,[3] Xuliang Chen,[1,2] Xuefei Wang,[2] Mingliang Tian,[1,5] Jian Sun,[6,5,†] Xiangang Wan,[3,5,‡] Zhaorong Yang,[1,2,5,§] Wenge Yang,[4,7,¶] Yuheng Zhang,[1,5] and Dingyu Xing[3,5]

[1] *High Magnetic Field Laboratory, Chinese Academy of Sciences, Hefei 230031, China*
[2] *Key Laboratory of Materials Physics, Institute of Solid State Physics, Chinese Academy of Sciences, Hefei 230031, China*
[3] *National Laboratory of Solid State Microstructures, College of Physics, Nanjing University, Nanjing 210093, China*
[4] *Center for High Pressure Science and Technology Advanced Research (HPSTAR), Shanghai 201203, China*
[5] *Collaborative Innovation Center of Advanced Microstructures, Nanjing University, Nanjing 210093, China*
[6] *National Laboratory of Solid State Microstructures, School of Physics, Nanjing University, Nanjing 210093, China*
[7] *High Pressure Synergetic Consortium (HPSynC), Geophysical Laboratory, Carnegie Institution of Washington, 9700 S Cass Avenue, Argonne, IL 60439, USA*

(Dated: August 31, 2016)

We report pressure-induced new phase in TaAs with different Weyl fermions than the ambient structure with aids of both theoretical calculations and transport/synchrotron structure investigations up to 53 GPa. We show that TaAs transforms from ambient $I4_1md$ phase (t-TaAs) to high-pressure hexagonal P-$6m2$ (h-TaAs) phase at 14 GPa, along with changes of electronic state from containing 24 Weyl nodes distributed at two energy levels to possessing 12 Weyl nodes at an iso-energy level, which substantially reduces interference between the surface and bulk states. The pressure-induced new phase can be reserved upon releasing pressure to ambient condition, which allows one to study the exotic behaviors of single set of Weyl fermions, such as the interplay between surface states and other properties.

PACS numbers: 61.50.Ks, 71.20.-b, 03.65.Vf, 71.90.+q

Weyl semimetal (WSM) is considered as three-dimensional (3D) analogs to graphene in terms of its electronic dispersion. One of the most striking characteristics of a WSM is the topological surface state with Fermi arcs. This was first proposed in pyrochlore iridates in 2011 [1] and extended to several other systems by different groups [2–5]. With the Weyl nodes behaving like Weyl fermions [1, 2] WSM possess novel transport properties stemming from the chiral anomaly [6–8]. Weyl nodes appear in pairs of opposite chirality due to the 'No-go theorem'. Recently, the non-centrosymmetric NbAs-type transition-metal monoarsenides, *i.e.* TaAs, TaP, NbAs, and NbP, have been predicted to be WSMs. Furthermore, all these four NbAs-type WSMs have twelve pairs of Weyl nodes in their 3D Brillouin zones [9, 10], and are completely stoichiometric and nonmagnetic, which provides a good platform for the novel property study in the topological WSMs. Soon after, many exotic properties associated with WSM have been observed, such as Weyl nodes, Fermi arcs [11–14] and the negative longitudinal magnetoresistance (MR) [15–17] due to the chiral anomaly [18–22]. These results demonstrate that TaAs family is a promising system that hosts topological properties, which might have potential applications in electronics, optoelectronics and quantum computing [23].

The 24 Weyl nodes in TaAs can be classified to two types, which locate at two different energy levels with considerable trivial Fermi pockets. The contribution from these trivial states complicates the analysis of topological surface states and novel transport behavior [10, 11]. Thus it would be interesting to find ways to reduce the number of Weyl nodes, degenerate them close to Fermi level, and consequently minimize the interference from the trivial states. High pressure has been considered as an effective and clean way to tune lattice as well as electronic states, especially in quantum states [24–26], thus it would be important to investigate the pressure effect on the Weyl nodes and size of the topological trivial Fermi surfaces.

In this Letter, we report a joint study of the evolution of the electronic and structural properties of single-crystal TaAs under high pressure, from both *ab initio* calculations and experimental measurements, including electrical resistance measurements and synchrotron X-ray diffraction (XRD) experiments. Our theoretical predictions and experimental results show that the Weyl nodes in the $I4_1md$ (t-TaAs) structure remain stable upon compression up to 14 GPa and a new P-$6m2$ (h-TaAs) phase with only one type of Weyl nodes emerges above 14 GPa. Upon decompression, this high-pressure h-TaAs phase can be kept to ambient pressure, which may allow one to study this new Weyl semimetal further at ambient conditions.

Theoretical calculation and experimental details are presented in Supplemental Material [27]. The ambient TaAs crystallizes in a body-centered tetragonal NbAs-

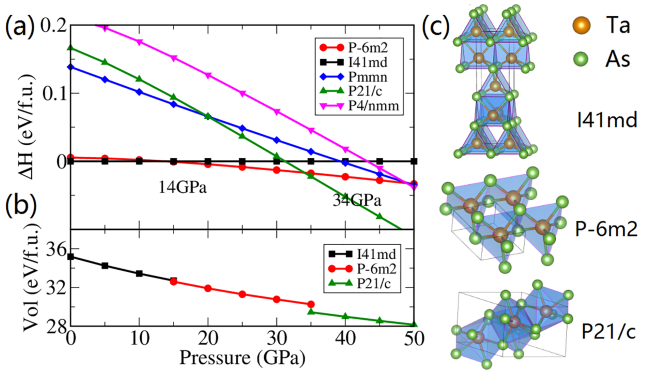

FIG. 1. (color online) (a) Calculated enthalpy relative to that of $I4_1md$ (t-TaAs) phase at pressure up to 50 GPa. (b) Unit cell volume vs. pressure. (c) Crystal structures of ambient phase (t-TaAs) and two best candidates of high-pressure phases (P-6m2 (h-TaAs) and $P2_1/c$ (m-TaAs)). Brown and green balls represent the Ta atom and As atom, respectively.

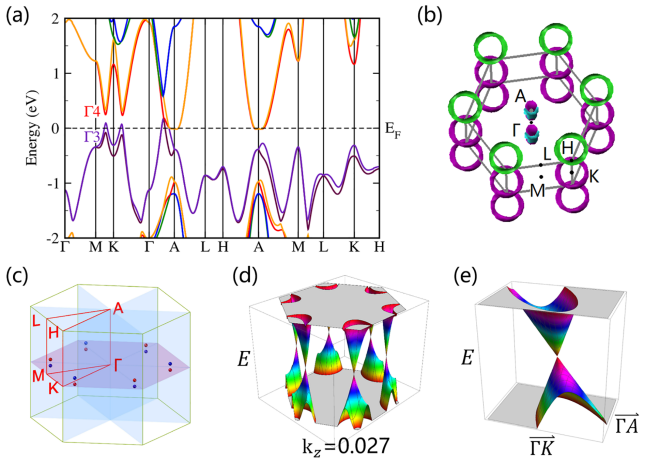

FIG. 2. (color online) Calculated electronic band structures of TaAs in h-TaAs phase at 25 GPa. (a) Electronic band structures with spin-orbit coupling. (b) Calculated Fermi surfaces of h-TaAs phase. (c) The Weyl nodes distribution in the first Brillouin Zone. The Weyl nodes obtained from scanning in the $k_z = 0.027$ plane (parallel to Γ-K-M) (d) and Γ-K-A plane (e), respectively.

type structure with the non-centrosymmetric space group $I4_1md$ ($D_{4\nu}^{11}$, No.109) [37], as shown in Fig. 1(c). The absence of a horizontal mirror plane in the unit cell breaks the inversion symmetry. It is known that the ambient t-TaAs structure has two kind of Weyl nodes. One type locates in the $k_z = 0$ plane (W1), and the other is off this plane (W2) [10, 11]. These two set of Weyl nodes have an energy difference about 14 meV at ambient pressure [11]. Pressure is utilized to tune these energy levels. As shown in Supplemental Table I, the Weyl nodes in t-TaAs phase are quite robust upon compression. We also calculated the band structures of t-TaAs phase at different pressures (see Supplemental Fig. S1). The overall shape of the band structure near Fermi level does not change much upon compression. With increasing pressure, the electron pockets become smaller while the hole pockets become larger, suggesting a multi-carrier system.

To check the energy favorite phases at higher pressure, we utilized crystal structure prediction techniques with the density functional theory (DFT) to calculate the enthalpy of all candidates of TaAs at each pressure. The enthalpy-pressure (ΔH-P) plots against the t-TaAs structure are shown in Fig. 1(a) at pressures up to 50 GPa. The ambient structure of TaAs is found to be t-TaAs, which is consistent with the experimental observations [37]. From 14 GPa to 34 GPa, the calculation predicts a h-TaAs structure has lower enthalpy than that of the t-TaAs structure. These two structures have the same type $TaAs_6$ polyhedron and a triangular prism with almost the same triangle side length and height, but different stacking sequences of the triangular prisms as shown in Fig. 1(c). The t-TaAs structure is constructed with AB sequence along the c-axis, while the h-TaAs structure has a uniform AA stacking. When the pressure reaches beyond 34 GPa, a $P2_1/c$ (m-TaAs) structure becomes the most energy favorite one. The crystal structure of the m-TaAs phase is nonmagnetic with inversion symmetry, thus Weyl nodes are no longer preserved. As shown in supplemental Fig. S2, the h-TaAs and m-TaAs phases are found to be dynamically stable at high and ambient pressure.

The band structure and Fermi surface of the high-pressure h-TaAs phase are calculated as shown in Fig. 2. The bands are overlapping near the A point which behaviors like a metallic phase, while the spin-orbit coupling opens a gap of around 160 meV for the crossing point near the K point. On the other hand, as shown in Supplemental Fig. S3(a) without SOC, there is a band inversion around K point. The hybridization between two bands belong two different irreducible representations is strictly forbidden, which results in the protected band crossing along K-Γ and K-M line and a gapless nodal ring around K point in the Γ-K-M plane.

The intriguing electronic structures of h-TaAs encourage us to investigate its topological properties. Interestingly, our calculations show that this non-centrosymmetric structure is also a Weyl semimetal. This phase has less Weyl nodes (12 in the 1st Brillouin Zone) as shown in Fig. 2(c). More interestingly, all these 12 Weyl nodes belong to the same type and are related with each other by symmetry, consequently they have the same energy. The Weyl nodes obtained from scanning in the k_z = 0.027 plane (parallel to Γ-K-M) and Γ-K-A plane are shown in Fig. 2(d) and (e), respectively. As presented in Supplemental Table II, the position of these Weyl nodes in h-TaAs structure stay almost unchanged, while the pressure has considerable effect on the position of Weyl nodes in the t-TaAs phase.

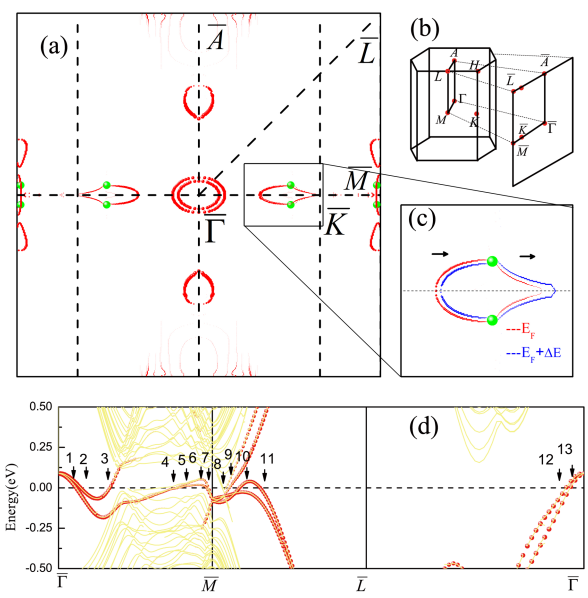

FIG. 3. (color online) Topological properties of TaAs in h-TaAs phase. (a) The surface state of As termination of TaAs in h-TaAs phase. Green dots are the bulk Weyl nodes projected to the 2D surface Brillouin zone. (b) The 3D Brillouin zone and the projected 2D surface Brillouin zone. (c) Evolution of the constant energy contour of two Fermi arcs. It can be seen that the two arcs move to the same direction as the energy shifts. (d) The band structure of (100) surface along closed loop ($\overline{\Gamma}$ - $\overline{M}$ - $\overline{L}$ - $\overline{\Gamma}$). The red dots are the surface electronic structure which projected to As termination.

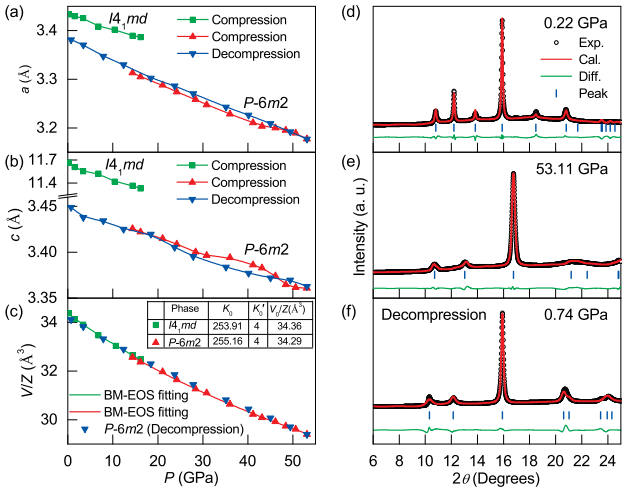

FIG. 4. (color online) High-pressure synchrotron XRD patterns of TaAs. Structural analysis reveals the irreversible phase transition $I4_1md$ (t-TaAs) to P-6m2 (h-TaAs) in TaAs upon decompression. (a) Lattice constant a, (b) lattice constant c, and (c) unit cell volume vs. pressure. Representative Rietveld refinements at (d) 0.22 GPa and (e) 53.11 GPa upon compression, respectively. (f) Pattern at 0.74 GPa upon decompression can be refined by the h-TaAs structure, suggesting that the high-pressure hexagonal phase is reserved.

To further investigate the topological properties of TaAs in the h-TaAs phase, we calculate the (100) surface state. The bulk Brillouin zone and the projected (100) surface Brillouin zone are shown in Fig. 3(b). One of the fundamental characteristic of the WSM is the existence of Fermi arcs [1]. There is a simple and effective way to verify the existence of nontrivial surface state [12–14]. We choose a generic closed loop in the 2D surface Brillouin zone, and count the number of Fermi surface crossings through this loop. The Fermi surface would cross the closed loop even times unless it is unclosed (Fermi arc). As shown in Fig. 3(a), we choose $\overline{\Gamma}$ - $\overline{M}$ - $\overline{L}$ - $\overline{\Gamma}$ as a closed loop to count the Fermi surface crossing. There are two Weyl nodes projected to the same point on the surface near $\overline{K}$ (Position 1, P1) and one Weyl node projected on the surface near $\overline{M}$ (Position 2, P2). Hence three Weyl points are enclosed in this loop. The number of Fermi surface crossing is expected to be odd. The surface band structure along $\overline{\Gamma}$ - $\overline{M}$ - $\overline{L}$ - $\overline{\Gamma}$ is illustrated in Fig. 3(d), the red dots are the surface states which are projected to As termination. We can count that the number of crossings is 13. This proves that the nontrivial surface states, Fermi arcs, exist on the (100) surface of TaAs.

The Fermi arcs can also be clarified by studying the evolution of the constant energy contours as a function of energy [11]. Two Fermi arcs move toward the same direction as one varies energy, while the trivial closed surface state would move to the opposite direction [11]. Figure 3(c) shows that the two Fermi surfaces around the P1 move to the same direction as the energy is increased by 20 meV. As a result, these two surface states become Fermi arcs.

To confirm the possible phase transition from the theoretical prediction, the TaAs sample was subjected to *in situ* high-pressure synchrotron XRD study. The angle-dispersive XRD experiments were conducted with diamond anvil cells up to 53.11 GPa. The powder diffraction profiles during compression and decompression are shown in Supplemental Fig. S4. The diffraction data clearly confirm the phase transition from t-TaAs phase to h-TaAs phase at 14 GPa. The evolutions of lattice parameter a, c and volume V/Z (unit cell volume per TaAs formula) up to 53.11 GPa are plotted in Fig. 4(a-c). It is clear that the long ordered structure along c axis in t-TaAs collapses to a similar lattice constant of hexagonal phase h-TaAs. We noticed the peak broadening of 10.5 degrees at 10.41 GPa, which indicates the settle in of the high-pressure phase. But the percentage of high-pressure phase is too low to fit reliable lattice parameters. So we call the transition pressure is 14.40 GPa thereafter. The detail GSAS Rietveld refinements at 0.22 GPa (pure t-TaAs phase), 16.15 GPa (mixture of t-TaAs and h-TaAs) and 53.11 GPa (pure high-pressure h-TaAs phase) show good fittings of the predicted structures (see Fig. 4 and Supplemental Fig. S5). Meanwhile, the structure of 0.74

GPa data obtained from the lowest decompression pressure shown in Fig. 4(f) can be refined by the h-TaAs structure, suggesting that the high-pressure hexagonal phase is reserved. Although the prediction of the transition pressure from t-TaAs to h-TaAs at 14 GPa is almost exact the same as XRD observations, up to 53.11 GPa we did not observe the second high-pressure phase transition from h-TaAs to m-TaAs predicted around 37 GPa. The t-TaAs and h-TaAs structures have the same $TaAs_6$ polyhedron but with different stacking sequences. Therefore, their enthalpies are very close to each other. In fact, the high-pressure synchrotron XRD experiments suggest that these two phases may coexist at pressures above the predicted critical pressure. In contrast, the m-TaAs phase consists of $TaAs_7$ polyhedron. The phase transition from the h-TaAs to m-TaAs needs large rearrangement of atoms, and breaking/reforming of chemical bonds, which can bring huge transition barrier and may hinder the transition from the h-TaAs to m-TaAs. However, with both inversion symmetry and time reverse symmetry, the m-TaAs phase cannot be a Weyl semimetal, which is out of current research interest.

In order to examine the effect of structural phase transition on the transport properties, we further performed the high-pressure resistance measurements. At ambient pressure TaAs exhibits a metallic-like behavior down to 2 K (see Supplemental Fig. S8). After applying external pressure of 1.1 GPa, the temperature dependence of resistance exhibits a semiconducting-like behavior ($d\rho/dT < 0$) over the entire measured temperature range, as shown in Fig. 5(a). The pressure-induced metal-semiconducting transition intuitively resembles the case of magnetic field effect on the resistance (see Supplemental Fig. S8(b)). Normally pressure enhances the band overlapping, the pressure-induced metal-semiconducting transition is indeed very unusual and not well understood yet. Similar phenomenon has been reported in other Dirac materials, such as Cd_3As_2 [38, 39], Bi_2Se_3 [40] and Sr-doped Bi_2Se_3 [41]. However, a common character in the Dirac materials is the high mobility of charge carriers. For example, the mobility of TaAs is 1.8×10^5 cm^2 V^{-1} s^{-1} at 10 K, which drops by almost 2 orders of magnitude upon warming to room temperature [16]. One possible reason for the semiconducting behavior under pressure is the suppression of mobility while carrier density changes little, similar to the case of Bi_2Se_3 [40]. This is because the mobility is very sensitive to the defects and stress induced by the pressure. From 1.1 to 10.0 GPa, the $R(T)$ curve keeps the semiconducting-like behavior. Nevertheless, this is not the case of isostructural NbAs, which remains metallic behavior up to 20 GPa [42]. The resistance at 300 K increases monotonically, while the resistance at 1.8 K first increases with pressure then decreases above 5.0 GPa (see Fig. 5(c)). Accordingly, when the pressure is increased to 14.0 GPa, a semiconducting-like to metallic-like transition emerges upon cooling, showing a resistance hump at T_{M-I} ~140 K. The hump in TaAs is very similar to the conduction of Dirac semimetal $ZeTe_5$ single crystal, where the resistivity anomaly could be attributed to the temperature-induced Lifshitz transition as recently revealed by angle-resolved photoemission spectroscopy (ARPES) measurements [43]. With further increasing pressure, the T_{M-I} shifts to higher temperatures.

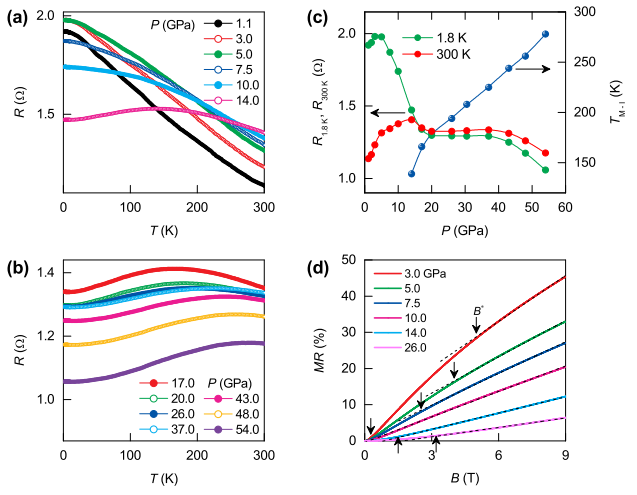

FIG. 5. (color online) Temperature dependences of resistance of a TaAs single crystal at various pressures. (a, b) Sample resistance profiles vs. temperature under high pressure. (c) The semiconductor-metal transition temperature T_{M-I} and specific resistance as a function of applied pressure at 1.8 K and 300 K, respectively. The T_{M-I} is defined as the hump on the resistance curve. (d) Isothermal magnetoresistance at 4.5 K under representative pressures. The dash lines denote the linear behavior. The arrows represent the characteristic magnetic field, B^*, below which the magnetoresistance deviates significantly from linearity.

Since TaAs possesses large MR in analogy to WTe_2 [44], which has been predicted very recently to be a new type of WSM [45], we investigated the MR at 4.5 K under different pressures. As shown in Fig. 5(d), no SdH oscillations up to 9 T can be observed after applying external pressure, which could be attributed to the suppression of mobility of charge carrier as discussed above. On the other hand, the MR is dramatically suppressed by pressure, which is similar to the case of pressurized WTe_2 [46, 47]. In WTe_2, the suppression of MR is accompanied by the emergence of superconductivity [47, 48]. However, in our case, no hint of resistance drop appears even down to 1.8 K till 54.0 GPa. Nevertheless, note that the MR curve at 10.0 GPa displays a linear behavior in a broad field region. As shown in Fig. 5(d), the characteristic field B^*, above which the linear MR is observed, first shifts monotonically to lower fields with increasing pressure from 3.0 GPa, then turns back for pressures above 10.0 GPa. Similar curvature change in the MR curve

has been observed in pressurized Ag_2Te due to pressure-induced crossover from p-type to n-type conductivity [49]. Combining with the fact that a semiconducting-like to metallic-like transition emerges upon cooling above 10.0 GPa, it can be deduced that this pressure is close to the critical pressure corresponding to the structural and topological phase transition as revealed by theoretical prediction and XRD results. The critical pressure close to 10.0 GPa is also revealed in Fig. 5(c), where the room-temperature resistance displays a maximum at 14.0 GPa, levels off in the pressure region from 20.0 to 37.0 GPa, and then drops slightly afterwards.

In summary, by combining theoretical and experimental investigations, we confirmed a new Weyl semimetal phase with a hexagonal lattice induced by pressure in TaAs at 14 GPa. Comparing to 24 Weyl nodes distributed at two different energy levels in the ambient tetragonal phase, high-pressure hexagonal phase is predicted to be a new topological semimetal with only 12 Weyl nodes at the same energy level. Decompression XRD experiments confirmed that the hexagonal phase is metastable at ambient pressure once it is formed beyond 14 GPa, which provides an excellent platform to study the interplay between surface states and other exotic properties without the limitation of access due to high pressure environments. As this is the first pressure-induced iso-energetic Weyl fermions in TaAs, further investigations on the novel surface electronic states and other possible exotic properties are desired.

Note added. During the review period of this work, the understanding of the electronic structures of this type of structure reaches a new level. We realize Weyl fermion and massless triply degenerate nodal points [50] coexist in our h-TaAs, similar to ZrTe [51]. Meanwhile, prediction for similar structures with a different method is reported [52]. Structures proposed by another work [53] seems do not fit to our experimental XRD data.

This research was financially supported by projects from the MOST of China (Grant Nos: 2016YFA0300404, 2015CB921202), the NSFC (Grant Nos: 51372112, 11525417, 11574133 and U1530402), NSF Jiangsu province (No. BK20150012), and the Fundamental Research Funds for the Central Universities and Special Program for Applied Research on Super Computation of NSFC-Guangdong Joint Fund (2nd phase). Part of the calculations was performed on the supercomputer in the High Performance Computing Center of Nanjing University. W. Y. acknowledges the financial support from DOE-BES X-ray Scattering Core Program under grant number DE-FG02-99ER45775. The XRD measurements were performed at the BL15U1 beamline, Shanghai Synchrotron Radiation Facility (SSRF) in China. The authors would like to thank Drs. Ke Yang and Shuai Yan for beamline technical support.

* These authors contributed equally to this work.
† jiansun@nju.edu.cn
‡ xgwan@nju.edu.cn
§ zryang@issp.ac.cn
¶ yangwg@hpstar.ac.cn

[1] X. Wan *et al.*, Phys. Rev. B **83**, 205101 (2011).
[2] G. Xu *et al.*, Phys. Rev. Lett. **107**, 186806 (2011).
[3] P. Hosur, Phys. Rev. B **86**, 195102 (2012).
[4] T. Ojanen, Phys. Rev. B **87**, 245112 (2013).
[5] A. C. Potter, I. Kimchi, and A. Vishwanath, Nat. Commun. **5**, 5161 (2014).
[6] A. A. Zyuzin and A. A. Burkov, Phys. Rev. B **86**, 115133 (2012).
[7] Z. Wang and S.-C. Zhang, Phys. Rev. B **87**, 161107(R) (2013).
[8] S. A. Parameswaran *et al.*, Phys. Rev. X **4**, 031035 (2014).
[9] S.-M. Huang *et al.*, Nat. Commun. **6**, 7373 (2015).
[10] H. Weng *et al.*, Phys. Rev. X **5**, 011029 (2015).
[11] S.-Y. Xu *et al.*, Science **349**, 613 (2015).
[12] B. Q. Lv *et al.*, Phys. Rev. X **5**, 031013 (2015).
[13] L. X. Yang *et al.*, Nat. Phys. **11**, 728 (2015).
[14] D. F. Xu *et al.*, Chin. Phys. Lett. **32**, 107101 (2015).
[15] C. Zhang *et al.*, arXiv:1502.00251.
[16] X. Huang *et al.*, Phys. Rev. X **5**, 031023 (2015).
[17] C. Shekhar *et al.*, arXiv:1506.06577.
[18] H. B. Nielsen and M. Ninomiya, Phys. Lett. B **130**, 389 (1983).
[19] V. Aji, Phys. Rev. B **85**, 241101(R) (2012).
[20] D. T. Son and B. Z. Spivak, Phys. Rev. B **88**, 104412 (2013).
[21] H.-J. Kim *et al.*, Phys. Rev. Lett. **111**, 246603 (2013).
[22] P. Hosur and X. Qi, C. R. Physique **14**, 857 (2013).
[23] D. Ciudad, Nat. Mater. **14**, 863 (2015).
[24] J. L. Zhang *et al.*, Proc. Natl. Acad. Sci. USA **108**, 24 (2011).
[25] C. Zhang *et al.*, Phys. Rev. B **83**, 140504(R) (2011).
[26] K. Kirshenbaum *et al.*, Phys. Rev. Lett. **111**, 087001 (2013).
[27] See Supplemental Material at http://link.aps.org/ supplemental/10.1103/PhysRevLett.xxx for the band calculation and experimental details and the supporting results, which includes Refs. [28–36].
[28] G. Kresse and J. Furthmller, Comput. Mater. Sci. **6**, 15 (1996).
[29] J. P. Perdew, K. Burke, and M. Ernzerhof, Phys. Rev. Lett. **77**, 3865 (1996).
[30] A. Togo, F. Oba, and I. Tanaka, Phys. Rev. B **78**, 134106 (2008).
[31] P. Blaha *et al.*, WIEN2k, An Augmented Plane Wave Plus Local Orbitals Program for Calculating Crystal Properties (TU Vienna, Vienna, 2001).
[32] J. Kuneš *et al.*, Phys. Rev. B **64**, 153102 (2001).
[33] A. P. Hammersley *et al.*, High Press. Res. **14**, 235 (1996).
[34] A. C. Larsen and R. B. Von Dreele, Los Alamos National Laboratory Report LAUR, 86 (2000).
[35] H. K. Mao, J. Xu, and P. M. Bell, J. Geophys. Res. **91**, 4673 (1986).
[36] C. Zhang *et al.*, arXiv:1503.02630.
[37] H. Boller and E. Parthé, Acta Cryst. **16**, 1095 (1963).
[38] S. Zhang *et al.*, Phys. Rev. B **91**, 165133 (2015).

[39] L. P. He *et al.*, arXiv:1502.02509.
[40] J. J. Hamlin *et al.*, J. Phys.: Condens. Matter **24**, 035602 (2012).
[41] Y. Zhou *et al.*, Phys. Rev. B **93**, 144514 (2016).
[42] J. Zhang *et al.*, Chin. Phys. Lett. **32**, 097102 (2015).
[43] Y. Zhang *et al.*, arXiv:1602.03576.
[44] M. N. Ali *et al.*, Nature **514**, 205 (2014).
[45] A. A. Soluyanov *et al.*, Nature **527**, 495 (2015).
[46] P. L. Cai *et al.*, Phys. Rev. Lett. **115**, 057202 (2015)
[47] X.-C. Pan *et al.*, Nat. Commun. **6**, 7805 (2015).
[48] D. Kang *et al.*, Nat. Commun. **6**, 7804 (2015).
[49] M. Lee *et al.*, Phys. Rev. Lett. **88**, 066602 (2002).
[50] H. Weng *et al.*, Phys. Rev. B **93**, 241202(R) (2016).
[51] H. Weng *et al.*, arXiv:1605.05186.
[52] M. Lu *et al.*, Solid State Commun. **240**, 37 (2016).
[53] J. Buckeridge *et al.*, Phys. Rev. B **93**, 125205 (2016).